Effect of concentration in Ge-Te liquids: A combined density functional and neutron scattering study

Matthieu Micoulaut, M.-V. Coulet, Andrea Piarristeguy, M. Johnson, Gabriel J. Cuello, C. Bichara, J.-Y. Raty, H. Flores-Ruiz, Annie Pradel

Effect of concentration in Ge-Te liquids: A combined density functional and neutron scattering study

M. Micoulaut,[1] M.-V. Coulet,[2] A. Piarristeguy,[3] M. R. Johnson,[4] G. J. Cuello,[4] C. Bichara,[5] J.-Y. Raty,[6] H. Flores-Ruiz,[1] and A. Pradel[3]

[1]*Laboratoire de Physique Théorique de la Matière Condensée, Université Pierre et Marie Curie, Boite 121, 4, Place Jussieu, 75252 Paris Cedex 05, France*

[2]*Aix-Marseille Université, CNRS, MADIREL UMR 7246, 13397 Marseille Cedex 20, France*

[3]*Institut Charles Gerhardt, UMR 5253-CNRS, Case 1503, Université Montpellier II, Place Eugène Bataillon, 34095 Montpellier Cedex 5, France*

[4]*Institut Laue Langevin, BO 156, 71, avenue des martyrs, 38042 Grenoble Cedex*

[5]*Centre Interdisciplinaire de Nanoscience de Marseille (CINaM), CNRS and Aix-Marseille Universities, Campus de Luminy, Case 913, 13288 Marseille, France*

[6]*Physique de la Matière Condensée, B5, Université de Liège, B4000 Sart-Tilman, Belgium*

(Received 15 February 2014; revised manuscript received 3 April 2014; published 30 May 2014)

The structural properties of three compositions of Ge-Te liquids ($Ge_{10}Te_{90}$, $Ge_{15}Te_{85}$, $Ge_{20}Te_{80}$) are studied from a combination of density functional based molecular dynamics simulations and neutron scattering experiments. We investigate structural properties including structure factors, pair distribution functions, angular distributions, coordination numbers, neighbor distributions and compare our results with experimental findings. Most noticeable is the good agreement found in the reproduction of the structure in real and reciprocal space, resulting from the incorporation of dispersion forces in the simulation. This leads to Ge and Te coordination numbers which are lower than in previous studies and which can now be followed with temperature, while also strongly depending on the chosen cutoff distance. Results show a gradual conversion of higher coordinated species (Te^{IV}, Ge^{V}) into lower coordinated ones at lower temperature, while leaving anticipated coordinations from the octet rule (Te^{II} and Ge^{IV}) nearly unchanged. Structural correlations are characterized as a function of temperature and composition. The vibrational density of states is also measured from inelastic neutron scattering for different compositions and temperatures, and compared to the simulated counterpart which exhibits a reasonable agreement at low frequency.

DOI: 10.1103/PhysRevB.89.174205 PACS number(s): 61.25.Em, 61.20.Ja, 71.15.Pd

I. INTRODUCTION

Due to their remarkable transparency in the infrared domain and their ability to be deposited in thin-film form, chalcogenide materials are of great interest for optoelectronic and computer science applications [1–3]. Some chalcogenide systems are classically studied, such as As-S [4,5], As-Se [6,7], or Ge-As-Se [8,9], although their transmission domain is limited in the long infrared wavelengths. Telluride materials have received an increased attention in the last years because this transmission domain can be extended up to 20 μm [10–12], and as some applications require microcomponents being able to work in an extended infrared domain such as spatial interferometry [13], biosensing, or environmental metrology [14], different Te-based systems have become particularly attractive, such as Te-Ge-I [1], Ge-As-Se-Te [15], Te-As-Se [16], or Ge-Ga-Te [17].

Another important application and source of intense research is related to the use of tellurides as phase-change materials for data storage in optical disks (DVD-RW) or phase-change memory (PCM) devices [18,19], the latter being an electrically driven data storage seen as a promising candidate for future nonvolatile memories [20]. In both applications, the data storage relies on the difference in optical or electronic properties between the crystalline and amorphous phases of the materials. Tellurides seem to bear the appropriate functionalities regarding such applications. Indeed, they possess low glass transition temperatures, low band gaps, stability of the crystalline and amorphous phases, different optical and electrical properties, and, finally, a fast recrystallization speed of the amorphous phase which enables designing appropriate setups regarding data storage.

However, from a more fundamental viewpoint, amorphous and liquid tellurides remain to be fully understood as even their structure is the subject of different interpretations [21,22]. But, other important and open issues are clearly identified.

First, many telluride alloys display in the liquid phase a certain number of anomalies. For instance, the existence of negative thermal expansions has been reported, and these are found over limited temperature ranges in, e.g., SeTe [23], STe [24], HgTe [25], In_2Te_3 [26], Ga_2Te_3 [26], As_2Te_3 [27], or Group-IV alloys (Si-Te [28] and Ge-Te [29]), and even in pure liquid tellurium [30] itself. There have been some recent computational [31,32] and experimental efforts [33,34] to understand the origin of this anomaly in elemental Te and in Ge-Te based alloys, some being based on either voids and rings [35] or on the investigation of small changes in the vibrational density of states with temperature [36]. Other anomalies related to density have been also reported such as a maxima in specific heat and sound velocity [28]. However, while some correlations with structural changes have been clearly identified [31,32], there is no consensus on the underlying driving force leading to the observed density anomaly.

Second, a certain number of computational studies using first-principles molecular dynamics (FPMD) and density functional theory (DFT) have been reported on, e.g.,

elemental Te [33] and on tellurium-based alloys containing a large amount of different alloying elements (Sb_2Te_3 [37], As_2Te_3 [38], GeTe [39–41]). However, in most of these studies, computed pair correlation functions or structure factors do not perfectly agree with corresponding experimental measurements from x-ray or neutron diffraction [31,42–44], and are certainly at a lower level of agreement when put in contrast with the same kind of study on lighter chalcogenides [45–47]. As a result, the bond distances and the coordination numbers are overestimated by at least 0.1 Å or 3%–4% while some uncertainty persists regarding the local neighborhood [48,49] of the Ge atom in, e.g., Ge-Sb-Te alloys, i.e., tetrahedral or octahedral. Alternative techniques have been proposed to refine the structure such as reverse Monte Carlo [50] or isochemical atomic substitution [51,52], but these deviate from the standard procedure of obtaining an amorphous system that is the cooling of a melt to lower temperature and its equilibration. More recently, semi-empirical dispersion forces have been taken into account in the exchange-correlation functional of FPMD and these have led to a substantial improvement of the structure in $Ge_{15}Te_{85}$ liquids [53]. A detailed analysis has shown that such dispersion forces indeed strongly affect the local geometry and first coordination shell of the atoms while bringing calculated coordination numbers closer to experimental findings [31,43]. We actually build on this approach in the present contribution.

Here, we report on the structural properties of three compositions in binary Ge-Te liquids ($Ge_{10}Te_{90}$, $Ge_{15}Te_{85}$, $Ge_{20}Te_{80}$) by combining neutron scattering measurements at three temperatures with a full analysis from DFT based simulations including dispersion forces. Except for the eutectic composition [31,32] ($Ge_{15}Te_{85}$), there have been only very few studies on Te-rich Ge-Te compositions in the literature, at least in the liquid state [42–44]. A systematic study with composition may therefore provide insight on how the addition of germanium atoms affects the chain network structure of elemental tellurium. This is the main purpose of the paper. Results show an agreement of very good quality when both the pair correlation function and the structure factor are compared to the experimental counterparts. Coordination numbers are found to be lower than those previously established [31,32]. It indicates that the well-known bond distance problem encountered in liquid and amorphous tellurides can be solved by using a phenomenological dispersion correction. The question of its effectiveness on amorphous structures is still open. This result actually goes well beyond methodological aspects, and has quite broad consequences for the field of phase-change materials. In this field, it has been stressed that the change from a crystalline to an amorphous structure may result from changes in local structure from a slightly distorted octahedral motif in the crystal [18,19] to a significant fraction of tetrahedral bonding in the amorphous phase. Since it is well known that octahedra usually share longer bonds as compared to tetrahedra [54], the obtained reduction of bond distances in the present systems potentially modifies the structural picture of liquids and amorphous tellurides while also challenging the nature of the underlying PCM phenomenon.

We finally calculate electronic properties, and compare vibrational properties of the liquid to the experimental measurements of the vibrational density of states (VDOS) from inelastic neutron scattering, and find a reasonable agreement at frequencies lower than 25 meV. A decomposition into partial contributions shows that the VDOS is made of two broad bands arising from Te and Ge, the former centered at 5 meV, while the latter is found to be at around 25 meV and shifts with increasing composition.

The paper is organized as follows. In Sec. II, we describe the experimental and numerical methods. In Sec. III, we present the experimental pair distribution functions and structure factors, and compare with the corresponding computed functions from simulations. In Sec. IV, we analyze the topology of the liquid structure as a function of temperature and composition by computing bond distances, average coordination numbers, bond angle distributions, coordination number distribution, and discuss the sensitivity of some of these findings with respect to the chosen cutoff distance. In Sec. V, we present the effect of temperature and composition on the electronic density of states, and compare the measured and computed VDOS. Finally, we summarize and draw some conclusions.

II. METHODS

A. Experimental methods

Three Ge-Te samples were investigated in this study and the exact compositions are given in Table I. The samples were prepared by direct alloying of high-purity ($4N$) elements. The materials (10 g) were synthesized by placing the powdered elements in stoichiometric proportions in a cylindrical silica ampoule (11 mm inner diameter, 1 mm thick). The sample-filled ampoules were evacuated to a pressure of about 10^{-5} mbar and sealed. Samples were then heated above their melting point at 10 K/h and homogenized for 8 h at $T = 800$ K in a furnace. The same samples were used for neutron diffraction and inelastic scattering experiments. Neutron diffraction experiments were performed on D4 instrument of the high-flux reactor at the Institute Laue Langevin (ILL, Grenoble, France). The incident neutron wavelength was fixed at 0.4976 Å using the Cu(220) Bragg reflection. The scattered intensities were measured through an ensemble of 9 moving detector banks (each of 64 cells) giving access to a k range of [0.4–23.5] $Å^{-1}$. A vanadium resistor was used as a furnace in order to perform the high-temperature measurements. The total structure factors $S_{expt}(k)$ were obtained after standard correction for background and container scattering, self-attenuation, multiple scattering, and inelasticity effects. The program CORRECT was used to perform the analysis [55]. The validity of the correction procedure was checked using the density values in the liquid state (see Table I) which were estimated by adjusting the mean differential scattering cross section per atom in the asymptotic limit [56]. Densities agree within less than 10% with the ones published by Tsuchiya [29]. Each sample was measured at three temperatures in the liquid state (see Table I) and the temperature accuracy was estimated to be around 10 K.

Inelastic neutron scattering experiments were carried out at a wavelength of 4.14 Å on the IN6 spectrometer at ILL. The $Ge_{15}Te_{85}$ sample was measured in the liquid state at 723, 823, and 923 K, while the $Ge_{20}Te_{80}$ sample was only studied at 723 and 923 K. A vanadium furnace was also used as the heating device and the temperature was determined within an accuracy

TABLE I. Experimental conditions (T_{expt}) and estimated densities ρ_{expt} in different liquid Ge tellurides: $Ge_{10}Te_{90}$, $Ge_{15}Te_{85}$, and $Ge_{20}Te_{80}$. Measured ratio $S_{expt}(k_2)/S_{expt}(k_1)$ of the first maxima at k_1 and k_2 of the experimental structure factor $S_{expt}(k)$, measured total coordination number N^{tot}_{expt} using the minimum r_m of the experimental pair correlation function $r^2 g_{expt}(r)$, calculated total coordination number N^{tot}_{th} from the simulated $g(r)$ (see text for details). Measured d_i^{expt} and calculated d_i^{th} first- ($i = 1$) and second- ($i = 2$) neighbor peak positions (in Å) of the total pair correlation function at different temperatures and compositions, together with calculated peak positions d_{ij}^{th} from the partial analysis (see also Fig. 5). Densities measured by Tsuchiya [29] are indicated.

	T_{expt} (K)	ρ_{expt} (Å^{-3})	$S = S_{expt}(k_2)/S_{expt}(k_1)$	N^{tot}_{expt}	r_m	N^{tot}_{th}	d_1^{expt}	d_1^{th}	d_2^{expt}	d_2^{th}	d_{ij}^{th}	i-j
$Ge_{10}Te_{90}$	923	0.0278(4)	0.81(2)	2.68(4)	3.22	2.37(5)	2.79	2.89	4.04	4.01		
		0.0273 [29]										
	823	0.0279(4)	0.81(2)	2.31(4)	3.12	2.19(8)	2.79	2.86	4.00	4.05		
		0.0277 [29]										
	703	0.0277(4)	0.85(2)	2.26(4)	3.10	2.09(3)	2.76	2.81	4.06	4.03		
		0.0283 [29]									2.46, 3.73	Ge-Ge
											2.67, 4.03	Ge-Te
											2.92, 4.11	Te-Te
$Ge_{15}Te_{85}$	913	0.0283(4)	0.82(2)	2.81(4)	3.22	2.36(8)	2.77	2.79	3.99	3.99		
		0.0282 [29]										
	833	0.0284(4)	0.82(2)	2.47(4)	3.13	2.20(2)	2.77	2.80	4.00	3.99		
		0.0286 [29]										
	683	0.0279(4)	0.90(2)	2.42(4)	3.11	2.06(4)	2.72	2.76	4.05	4.02		
		0.0292 [29]									2.54, 3.78	Ge-Ge
											2.68, 4.02	Ge-Te
											2.95, 4.02	Te-Te
$Ge_{20}Te_{80}$	923	0.0282(4)	0.83(2)	2.96(4)	3.24	2.35(9)	2.78	2.76	3.97	4.03		
		0.0291 [29]										
	823	0.0284(4)	0.83(2)	2.64(4)	3.15	2.14(2)	2.76	2.74	4.00	4.01		
		0.0296 [29]										
	703	0.0280(4)	0.86(2)	2.51(4)	3.12	2.12(9)	2.73	2.73	4.02	3.97		
		0.0302 [29]									2.57, 3.82	Ge-Ge
											2.70, 3.97	Ge-Te
											2.94, 4.06	Te-Te

of 20 K. The standard corrections were applied to the data. They consist in normalizing the spectra to identical values, substracting of the container contribution, and normalizing to a reference spectrum of an 11-mm-diameter vanadium cylinder. The data were corrected for the energy-dependent detector efficiency and time-independent background. Afterwards, the time-of-flight data were converted into a dynamical structure factor $S_{expt}(2\theta,\omega)$. First, an integration of $S_{expt}(2\theta,\omega)$ over the accessible ω range was done to obtain the structure factor $S_{expt}(k)$ over a k range between 0.31 and 2.56 Å^{-1} and, thus, checked the validity of the container subtraction that strongly contributes to the signal. Second, an integration of $S(2\theta,\omega)$ over the 2θ range accessible to the experiment (11.9° to 114.9°) was performed in order to obtain the VDOS $g(\omega)$. All the correction procedure was done using the LAMP program [57]. As already highlighted in our previous studies [36], since the k range available to the experiment is finite and correlated with the ω range, the density $g(\omega)$ is incomplete and slightly distorted. However, since the (k,ω) range was the same for all measurements, it is reasonable to compare the various VDOS obtained.

B. Computational details

FPMD simulations (CPMD code) have been performed at constant volume on systems containing 200 atoms (Fig. 1) positioned in a periodically repeated cubic cell whose size allows recovering the experimental densities of the liquid. The electronic structure has been described within density functional theory (DFT) [58]. A generalized gradient approximation was used, using an improved scheme for the exchange-correlation energy obtained by Perdew, Burke, and Ernzerhof (PBEsol)

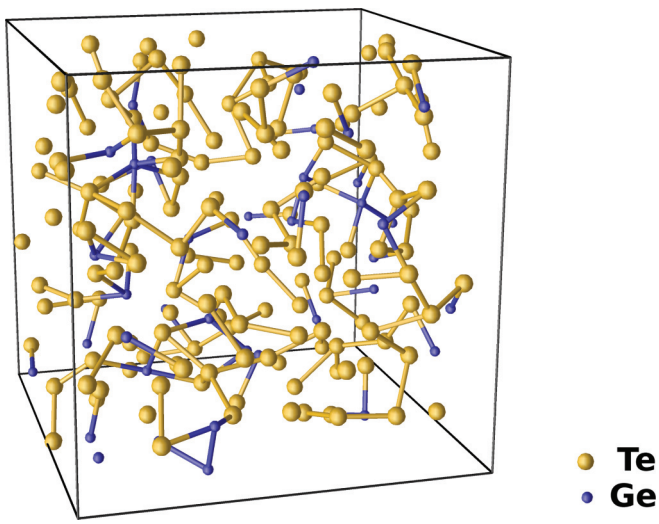

FIG. 1. (Color online) A snapshot of the 200-atoms liquid $Ge_{20}Te_{80}$ at 923 K.

previously used for the study of elemental tellurium [33]. Valence electrons were treated explicitly, in conjunction with Trouiller-Martins norm-conserving pseudopotentials [59]. The wave functions have been expanded at the Γ point of the supercell on a plane-wave basis set with an energy cutoff $E_c = 20$ Ry. During the Car-Parrinello molecular dynamics (CPMD) simulation, a fictitious electron mass of 2000 a.u. and a time step of $\Delta t = 0.12$ fs has been used to integrate the equations of motion. Temperature control has been implemented for both the ionic and electronic degrees of freedom by using Nosé-Hoover thermostats [60] with a frequency of 800 cm^{-1}.

In addition, we have used an (attractive) empirical dispersion coefficient (Grimme) correction [61] given by

$$E_{\rm disp} = -s_6 \sum_{i=1}^{N-1} \sum_{j=i+1}^{N} \frac{C_{ij}}{R_{ij}^6} f_{dmp}(R_{ij}), \qquad (1)$$

where N is the number of atoms of the system, C_{ij} is the dispersion coefficient for atom pair ij, and R_{ij} is the interatomic distance. A damping function [61] $f_{dmp}(R_{ij}) = (1 + \exp[-d(R_{ij}/R_c - 1)]^{-1}$ has been also used in order to avoid singularities at short interatomic distances. Here, R_c is a cutoff distance canceling $E_{\rm disp}$ for $R < R_c$. Parameters for the Ge-Te systems (R_c, C_{ij}, d_{ij}) are given in Ref. [53]. However, a major drawback is the fact that these calculations are not self-consistent and contain adjustable parameters that correct the energy of a DFT converged calculation. One has, thus, to keep in mind that such simulations can not be considered as deriving from first principles, and may also depend on the chosen parameters as emphasized in a recent study on liquid water [62].

For comparison, simulations without the dispersion forces have been performed under the same thermodynamic conditions, and will serve in the discussion.

The starting configuration of all liquids is a random structure of Ge and Te atoms fulfilling the desired stoichiometry. Loss of the memory of this initial configuration is achieved through preliminary runs at 2000 and 1500 K over 50 ps at densities corresponding to a high-temperature extrapolation of the experimental density [29] to ensure $P \simeq 0$. The experimentally measured densities (Table I) were then chosen for the investigated isotherms. The chosen time interval leads to corresponding mean-square displacements of the order of several cell lengths. After equilibrating at the three target temperatures (923, 823, and 700 K) over 5 ps, trajectories for each composition have been accumulated over 25 ps each and used for the statistical analysis. The obtained structure (e.g., Fig. 1) reveals the presence of various structural motifs (including homopolar Ge-Ge and Te-Te bondings) and coordinations that are characterized in detail.

III. QUALITATIVE ANALYSIS OF THE DATA

A. Global trends in the experimental data

The experimental total structure factors $S_{\rm expt}(k)$ for the three compositions are presented in Fig. 2 for each temperature. At a given composition, temperature increase results in an overall damping of the k or r oscillations, but noticeable changes between low and intermediate temperatures are observed. Upon temperature increase, peak positions in

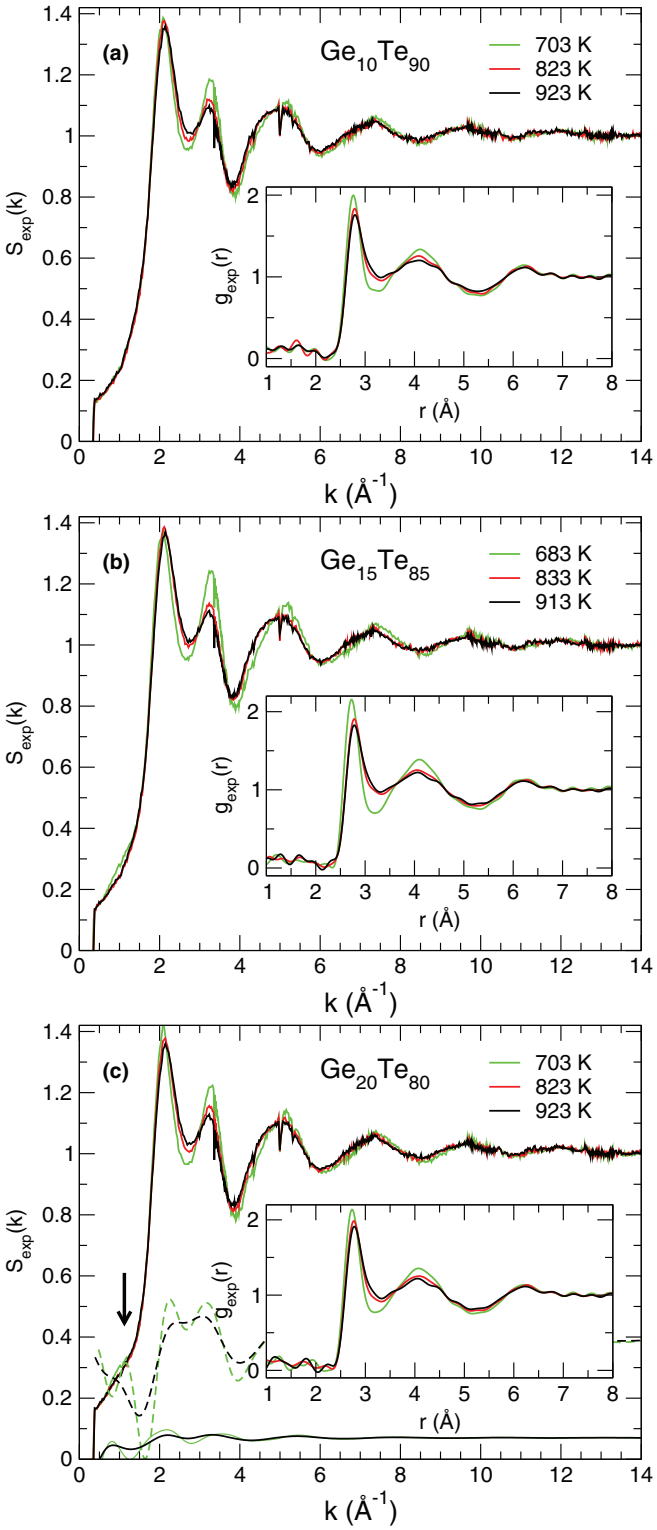

FIG. 2. (Color online) Experimental total structure factor $S_{\rm expt}(k)$ for three compositions $Ge_{10}Te_{90}$ (a), $Ge_{15}Te_{85}$ (b), and $Ge_{20}Te_{80}$ (c) measured at three temperatures. The corresponding total pair correlation function $g_{\rm expt}(r)$ are presented as insets. In panel (c), the decomposition from simulation in the partials $S_{\rm GeGe}(k)$ (solid curves) and $S_{\rm GeTe}(k)$ (broken curves) is shown for 700 K (green) and 923 K (black). The arrow indicates the tiny shoulder observed experimentally [also seen in panel (b) at the lowest temperature, green curve].

$S_{expt}(k)$ are slightly shifted towards smaller k values, except for the first peak (located around 2.1 Å^{-1}) that shows an opposite behavior. This indicates that the observed changes in the total structure factors are not only linked to thermal disorder but also due to some structural modifications in the liquid. These results are in agreement with previous experimental work performed on the $Ge_{15}Te_{85}$ liquid alloys [33]. We furthermore note that the temperature effect is more important at the eutectic composition for which the density anomaly is the more pronounced [29].

It is possible to define an order parameter $S = S(k_2)/S(k_1)$ that allows distinguishing between an octahedral liquid ($S < 1$, $Ge_{15}Te_{85}$ for instance) and an tetrahedral one ($S > 1$, $GeSe_2$ for instance) [63]. Values of this parameter are reported in Table I. For all compositions, S is lower than 1 suggesting that the present liquids display a globally octahedral local order as also detailed below from the simulation results. However, it can be noted that S increases with decreasing temperature, which suggests an increased tendency to form tetrahedral geometries at low temperature.

Finally, for $Ge_{15}Te_{85}$ and $Ge_{20}Te_{80}$, a small shoulder is observed around 1.1 Å^{-1} on the measured $S_{expt}(k)$ at the lower temperature (683–703 K). Such a contribution suggests structural rearrangements in the medium range order, and it corresponds to a pseudoperiodicity at distances around $7.7/k = 7$ Å in real space [64]. The onset of this tiny shoulder is linked to the increase of Ge content as revealed by the calculated partial structure factors $S_{ij}(k)$ which show an increased contribution at 1.12 Å^{-1} of the Faber-Ziman partial structure factor $S_{GeTe}(k)$ for $Ge_{20}Te_{80}$ at the lowest temperature [703 K, Fig. 2(c)]. This observation is reinforced by the fact that the positions of the two principal peaks (PPs) at k_1 and k_2 vary slightly with composition: the first peak shifts to higher wave vector between 10% (2.13 Å^{-1}) and 15% Ge (2.18 Å^{-1}) for, e.g., 923 K (or lower temperatures). Since this observation can not be attributed to an important change in liquid density (Table I), it must therefore be linked to the occurrence of weaker long-range correlations as the Ge content increases. Interestingly, this contribution is immediately damped when the temperature is increased as observed for the eutectic composition [33]. Amorphous Ge-Te alloys at various Ge content around the eutectic composition also possess [50,65] a small prepeak around 1 Å^{-1}, and it has been proposed that Ge atoms play a dominant role in this medium range order [50].

The corresponding total pair correlation functions $g_{expt}(r)$ [Fourier transform of $S_{expt}(k)$] are presented as insets in Fig. 2 for each temperature. Here, again, major changes occur between the lowest (683–703 K) and the other temperatures. With increasing temperature, the first peak height decreases, and the minimum at $r \simeq 2.5$–2.8 Å defining the first and second shells of neighbors tends to disappear. This underscores a less structured liquid at high temperature. Moreover, the first-neighbor distance d_1^{expt} increases with temperature (from, e.g., 2.76 to 2.79 Å in $Ge_{10}Te_{90}$, Table I), while the second-neighbor distance d_2^{expt} slightly decreases (e.g., from 4.02 to 3.97 Å in $Ge_{20}Te_{80}$), leading to a more compact local environment.

Using these total pair correlation functions and the experimentally determined densities (see Table I), it is possible to obtain a total coordination number N_{expt}^{tot} defined by

$$N_{expt}^{tot} = 4\pi\rho_{expt}\int_{r_0}^{r_m} r^2 g_{expt}(r)dr, \quad (2)$$

the lower integration bound r_0 being fixed to 2.2 Å for all the spectra (see insets of Fig. 2). The values of the upper bound r_m (given in Table I) are chosen as the value of the first minimum r_m of the function $r^2 g_{expt}(r)$. We emphasize that N_{expt}^{tot} has no real physical meaning since a binary alloy is studied here, however, it can be used as an indicator of the average structural changes undergoing as the temperature and the Ge content are changed. As seen in Table I, N_{expt}^{tot} increases with increasing the Ge concentration, which is a rather expected result since, on average, the addition of a Group-IV atom (Ge) leads to an increase in coordination number and network connectivity. Moreover, N_{expt}^{tot} also increases gradually with temperature which is consistent with previous studies on the liquid structure at the eutectic composition [33,34], indicating that the coordination number of Te is increasing with temperature.

B. Effect of the dispersion forces on the simulated data

In Fig. 3, we represent a direct comparison of the experimental total structure factors (same as Fig. 2) with the corresponding computed neutron-weighted function $S_T(k)$ defined by

$$S_T(k) = \frac{\sum_{i,j} c_i c_j b_i b_j S_{ij}(k)}{\left(\sum_{i,j} c_i b_i\right)^2}, \quad (3)$$

where the concentrations c_i (i = Ge, Te) depend on the chosen stoichiometry (e.g., $c_{Ge} = 0.10$, 0.15, and 0.20 for $Ge_{10}Te_{90}$, $Ge_{15}Te_{85}$, and $Ge_{20}Te_{80}$, respectively), and b_i are the neutron scattering lengths given by $b_{Ge} = 8.185$ fm and $b_{Te} = 5.68$ fm, respectively [66]. The Faber-Ziman partials $S_{ij}(k)$ have been directly computed from the simulated trajectory (see, e.g., Fig. 2). From the figures, one realizes that the calculated spectra reproduce rather well the experiments over the whole range of wave vectors, for all temperatures and compositions, all curves being nearly superimposed for $k \leqslant 6$ Å^{-1}. This agreement is also evidenced from the represented interference function $I(k) = k[S_T(k) - 1]$ which blows up the oscillations at higher k value [Fig. 3(c)] and provides confidence that real-space properties at short distance r ($r \propto 1/k$) should be also reasonably well reproduced. We furthermore note that the presence of dispersion forces [Eq. (1)] leads to a substantial improvement of the structure factor at different conditions and increasing Ge composition, the $Ge_{20}Te_{80}$ showing the best agreement with experimental data. Note that the absence of such dispersion forces leads to a shift towards low-k values of the peak found at $\simeq 5.5$ Å^{-1} [green curve for $Ge_{10}Te_{90}$, see Fig. 3(c)], and the high wave-vector region appears to be not very well reproduced.

We now turn to real-space properties. In Fig. 4, we represent the calculated total pair correlation function $g(r)$ for the different compositions and temperatures. The agreement appears to be very good, and again, clearly improved with respect to previous simulations [31,32] on selected compositions (mostly $Ge_{15}Te_{85}$). The first peaks experimentally observed

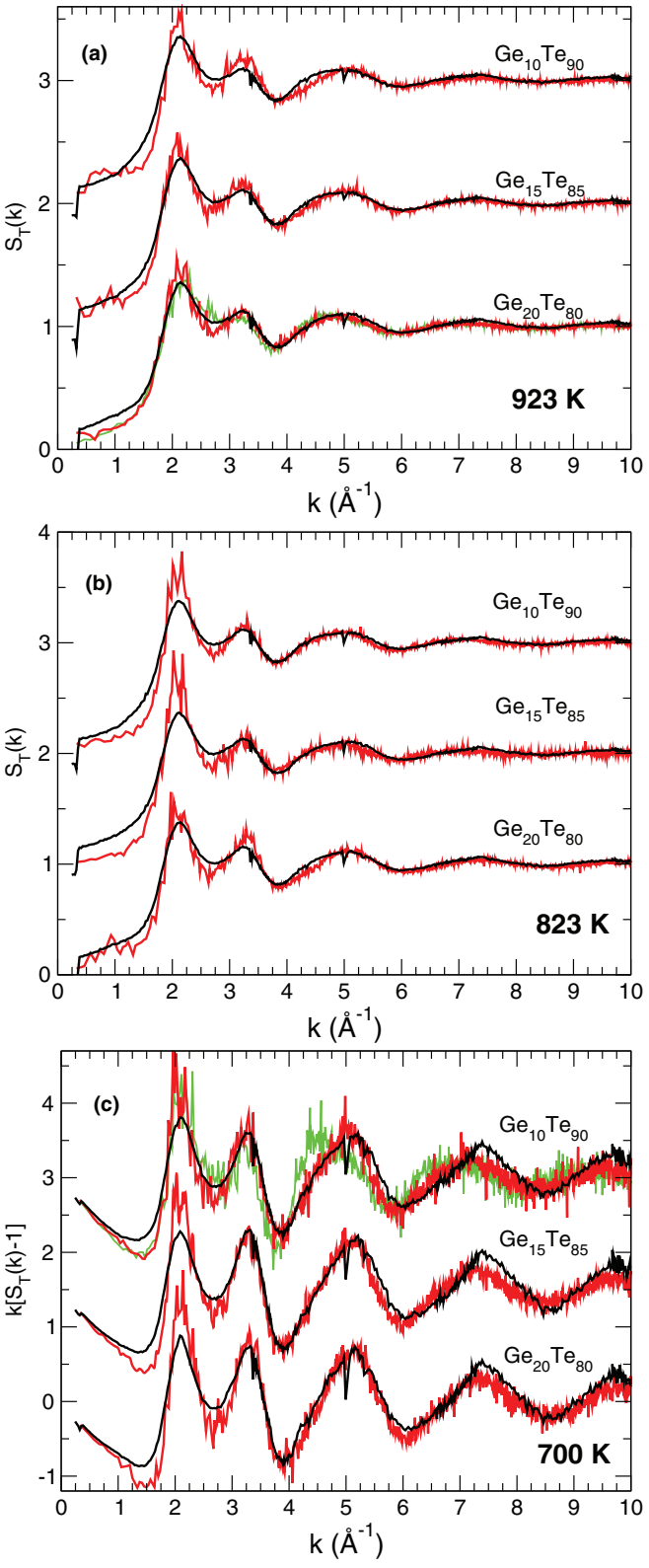

FIG. 3. (Color online) Calculated total neutron structure factor $S_T(k)$ (a), (b) and interference function $k[S_T(k) - 1]$ (c) in Ge-Te liquids for three compositions $Ge_{10}Te_{90}$, $Ge_{15}Te_{85}$, and $Ge_{20}Te_{80}$ and three temperatures (700, 823, and 923 K, red curves) compared to results from neutron diffraction (black curves, same as Fig. 2). The green curves correspond to similar simulation conditions but without taking into account the dispersion forces of Eq. (1) (see text for details).

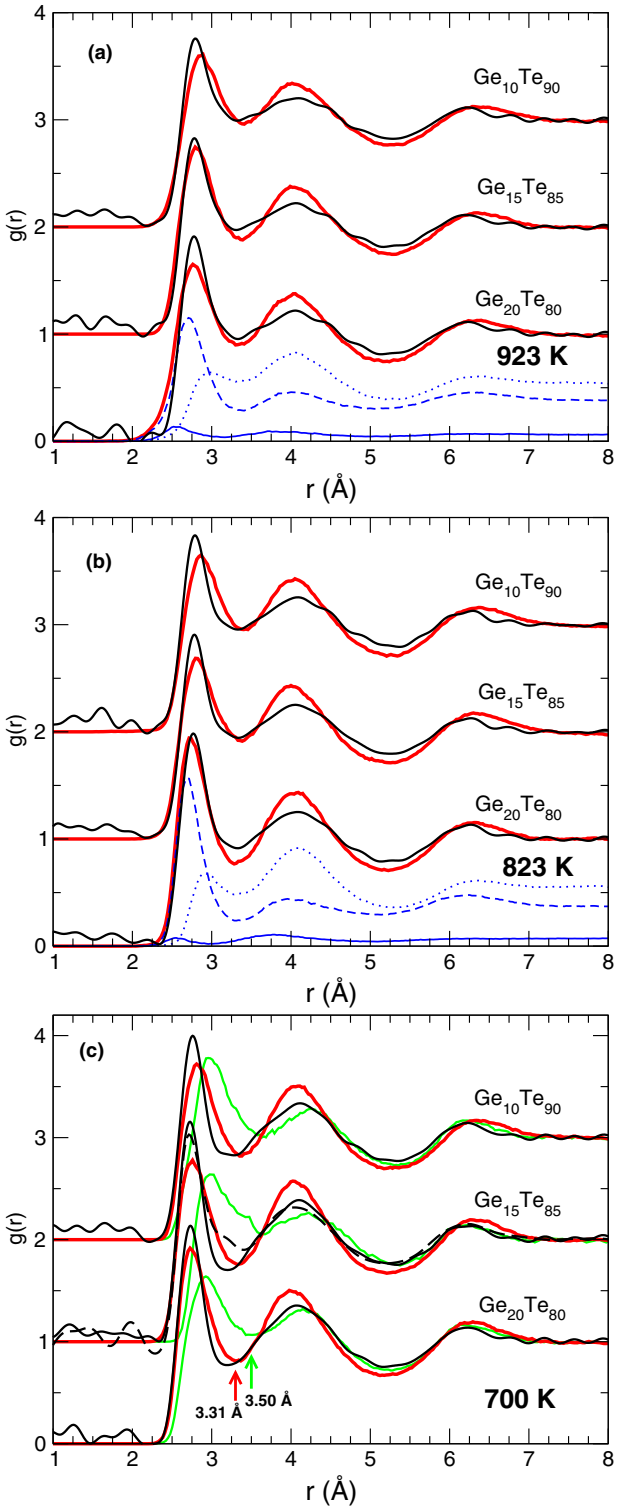

FIG. 4. (Color online) Calculated total pair distribution functions $g(r)$ for three compositions $Ge_{10}Te_{90}$, $Ge_{15}Te_{85}$, and $Ge_{20}Te_{80}$ and three temperatures (700, 823, and 923 K, red curves) compared to results from neutron diffraction (solid black curves, same as Fig. 2, and broken curve [31]). In panels (a) and (b), a decomposition into partials (blue curves) is shown for the $Ge_{20}Te_{80}$ alloy: Ge-Ge (solid curve), Ge-Te (broken curve), Te-Te (dotted curve). In panel (c), green curves correspond to simulations without the dispersion forces [Eq. (1)]. The arrows indicate the position r_{min} of respective minima in $Ge_{20}Te_{80}$ (see text for details).

at $r \simeq 2.77$–2.79 Å and at $r \simeq 4$ Å are very well reproduced from our simulations for all systems (Table I), both positions d_1^{th} and d_2^{th} of the main peaks, and peak height being in very good agreement. Furthermore, simulations display the same structured pair correlation function as in experiments [31], revealed by a more pronounced minimum (with respect to simulations without Grimme correction, see green curves) in the 3.28–3.42 Å range, which leads to a rather well-defined separation between the first and second shell of neighbors. For the $Ge_{15}Te_{85}$ liquid, the minimum of the simulated $g(r)$ at 700 K actually lies between two sets of experimental measurements: the present one performed at 683 K, and a previous measurement by Bergman *et al.* [31] at 733 K.

A closer inspection shows that the agreement is increased with Ge composition, the position of first peak in the simulated $g(r)$ for $Ge_{10}Te_{90}$ being slightly overestimated (2.81 Å against 2.76 Å experimentally at 703 K, see Table I). This situation tends to be improved as the Ge composition is increased, the first peak position being identical with the experimental counterpart for $Ge_{20}Te_{80}$ (2.73 Å at 703 K). Again, we attribute this improved agreement with increasing Ge composition to the effect of the dispersion forces which take into account the polarizability [61]. The latter is obviously affected by the increased presence of heteropolar Ge-Te bonds which involve atoms having different electronegativities (2.1 and 2.01 for Te and Ge on the Pauling scale [67]). This in turn gives rise to the possibility of having an increased number of dipolar interactions and an increased effect due to (Van der Waals) dispersion forces.

Simulations without such dispersion forces show indeed a systematic deviation of the main peak of the pair correlation function [green curves, Fig. 4(c)] which is being shifted to larger distances by $\simeq$0.2 Å. This effect is observable for all compositions, and at all temperatures (not shown). The same behavior is obtained for the position of the first minimum which is also shifted to higher distances. For $Ge_{20}Te_{80}$ at 700 K, the minimum position is actually increased from $r_{\min} = 3.31$ Å to $r_{\min} = 3.50$ Å [arrows in Fig. 4(c)] if dispersion forces are not taken into account. One can already anticipate that corresponding coordination numbers will be increased given that they are usually calculated from the integration of the pair correlation function up to this first minimum [Eq. (2)]. Using the latter, the computation of the total coordination number N_{th}^{tot} from the calculated $g(r)$ (Table I) shows a similar decrease with temperature when compared to the experimental estimate of N_{th}^{tot}, although differences persist in the absolute value which arise from the small differences between simulated and experimental pair correlation functions (Fig. 4). Interestingly, we note that the improvement of the calculated $g(r)$ is especially pronounced at low distance ($r < 3.5$ Å) where the effect of the dispersion forces is not active given that the damping function f_{dmp} in Eq. (1) cancels for distances below the cutoff distance $R_c = 3.45$ Å (see Ref. [53]). It thus suggests that taking into account Eq. (1) implies the presence of attractive Van der Waals forces which must result in more closely connected long-range correlations at $r > R_c$ and should therefore affect second and third shells of neighbors as revealed by the different structure factors [Fig. 3(c)]. Surprisingly, this difference does not show up at large distance in the pair correlation function as both simulations lead to an identical result for $r > 4$ Å.

The calculation of the partial pair correlation function shows that the main contribution to the first peak found at $r \simeq 2.77$–2.79 Å arises from Ge-Te bonds (blue broken curve in Fig. 4), whereas the second peak is mostly due to second-neighbor Te-Te correlations which are, in part, due to Te interchain distances (3.2–3.7 Å) remaining from the initial Te base network [33,68]. For the Ge-rich composition ($Ge_{20}Te_{80}$), a non-negligible amount of homopolar Ge-Ge bonds is revealed by the presence of contribution in the partial g_{GeGe} which is also detectable at Ge-poor compositions.

IV. TOPOLOGY OF THE LIQUID

We now concentrate on the partial coordination numbers of germanium and tellurium and their evolution with composition and temperature.

A. Coordination numbers

From the obtained simulated pair correlation functions (Fig. 5), we obtain by integrating up to corresponding first minima $r_{\min}$ the partial coordination numbers n_{GeGe}, n_{TeGe}, and n_{TeTe} for the different compositions and temperatures (Table II) using

$$n_{ij} = 4\pi\rho \int_0^{r_{\min}} r^2 g_{ij}(r) dr. \tag{4}$$

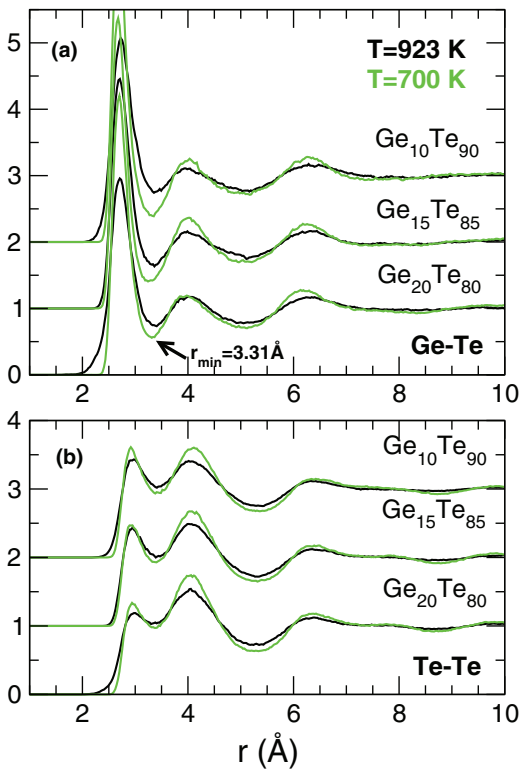

FIG. 5. (Color online) Calculated partial pair distribution functions $g_{\text{GeTe}}(r)$ and $g_{\text{TeTe}}(r)$ for three compositions $Ge_{10}Te_{90}$, $Ge_{15}Te_{85}$, and $Ge_{20}Te_{80}$ and two temperatures: 923 K (black curve) and 700 K (green curve). The arrow indicates the position (3.31 Å) of the minimum at 700 K (see text for details).

TABLE II. Calculated partial coordination numbers n_{GeGe}, n_{TeGe}, and n_{TeTe}, coordination numbers n_{Ge} and n_{Te}, and average coordination number $\bar{r}$ at different temperatures in $Ge_{10}Te_{90}$, $Ge_{15}Te_{85}$, and $Ge_{20}Te_{80}$ liquids. All calculations have been computed at the corresponding minimum of the relevant partial pair correlation function [e.g., $r_{min} = 3.31$ Å in $g_{GeTe}(r)$ for a 700-K liquid $Ge_{20}Te_{80}$, see Fig. 4]. Numbers are given with an error bar of ±0.1.

T (K)	Composition	n_{GeGe}	n_{TeGe}	n_{TeTe}	n_{Ge}	n_{Te}	$\bar{r}$
923 K	$Ge_{10}Te_{90}$	0.11	0.46	2.87	4.25	3.34	3.42
823 K		0.10	0.47	2.82	4.33	3.29	3.39
700 K		0.03	0.47	2.53	4.26	3.00	3.13
923 K	$Ge_{15}Te_{85}$	0.38	0.71	2.57	4.40	3.28	3.44
823 K		0.21	0.76	2.57	4.52	3.32	3.51
700 K		0.34	0.68	2.40	4.19	3.08	3.24
923 K	$Ge_{20}Te_{80}$	0.52	0.98	1.96	4.45	2.94	3.24
823 K		0.23	1.02	1.76	4.30	2.77	3.08
700 K		0.34	1.01	1.88	4.37	2.89	3.19

Note that one has $(1-x)n_{TeGe} = xn_{GeTe}$ with x the Ge concentration (e.g., $x = 0.2$ in $Ge_{20}Te_{80}$). Results indicate that a change from $Ge_{10}Te_{90}$ to $Ge_{20}Te_{80}$ leads, as expected, to a decrease of the n_{TeTe} partial coordination number while an increase of n_{TeGe} is obtained upon Ge addition. From such numbers, the Ge and Te coordination numbers can be computed as a function of temperature by $n_{Ge} = n_{GeGe} + n_{GeTe}$ and $n_{Te} = n_{TeTe} + n_{TeGe}$. General trends can be established although it is important to emhasize that the evolution of the partials g_{ij}(r) around $r = r_{min}$ leads to variations in n_{ij} and n_i that are driven by the uncertainties on r_{min}. A detailed analysis on the effect of the cutoff distance is therefore reported below.

Along the isotherm at 700 K n_{Te} decreases with increasing Ge content, from 3.00 (respectively 3.34 for 923 K) for $Ge_{10}Te_{90}$ to 2.89 (respectively 2.94) for $Ge_{20}Te_{80}$. This also leads to a decrease of the connectivity $\bar{r}$ of the liquid defined by $\bar{r} = (1-x)n_{Te} + xn_{Ge}$ which remains nearly unaffected by the change in composition between 10% and 15% Ge. The situation is more ambiguous for n_{Ge} which is found to either decrease or increase with temperature and/or composition, e.g., steadily increasing with Ge content at high temperature (from 4.30 to 4.45 at 923 K). For the latter system, the results at 700 K are found to be very close to those obtained from a similar analysis (680 K) which yields [32] partial coordination numbers $n_{TeGe} = 0.6$ (here 0.68, see Table II), $n_{TeTe} = 2.5$ (2.40), to finally obtain $n_{Ge} = 3.7$ (here 4.17) and $n_{Te} = 3.1$ (3.08). It should be stressed that the chosen cutoff (3.2 Å in Ref. [32]) for the calculation of the coordination numbers was lower than the reported minimum in the pair distribution function (3.3–3.4 Å). We discuss effects of the cutoff distance below. Similar results have been obtained in Refs. [31,69] from a structural analysis of $Ge_{15}Te_{85}$ at different temperatures around 700 K.

B. Effect of the cutoff distance

To investigate further the effect of a chosen cutoff distance on the calculation of coordination numbers, we represent the most relevant running coordination number (n_{GeTe}) as a function of the interatomic distance (Fig. 6) for different

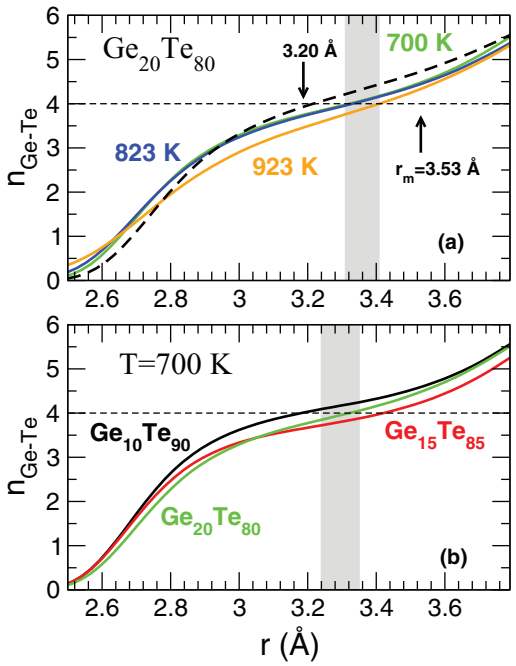

FIG. 6. (Color online) Running Ge-Te coordination number as a function of interatomic distance, calculated from the integration of the function $r^2 g_{GeTe}(r)$. (a) Effect of temperature (923, 823, and 700 K) on $Ge_{20}Te_{80}$. (b) Effect of composition on the 700-K liquid: $Ge_{10}Te_{90}$ (black), $Ge_{15}Te_{85}$ (red), and $Ge_{20}Te_{80}$ (green). The gray areas correspond to the zones where g_{GeTe} is minimum (see arrow in Fig. 5). Horizontal broken lines correspond to $n_{GeTe} = 4$ and serve as a guide. The broken curve in (a) represents results from a simulation without the dispersion forces, and the arrows indicate either the cutoff needed to obtain $n_{GeTe} = 4$ (3.20 Å), or the location of the minimum ($r_{min} = 3.53$ Å) of the corresponding partial pair distribution function $g_{GeTe}(r)$.

compositions and temperatures. As shown from the figure, $n_{GeTe}(r)$ changes continuously with r, and does not display a plateaulike behavior typical of amorphous systems [70] or liquids with well-separated neighbor shells. As a result, a slight shift in cutoff will strongly affect the value of the coordination itself, the variation being also important within the r_{min} distance interval (gray zones in Fig. 6) for which the different $g_{GeTe}(r)$'s are minimum (e.g., arrow in Fig. 5). This effect appears to be even more important when the liquids are considered along an isotherm [Fig. 6(b)] given the way r_{min} is changed with composition.

For the $Ge_{20}Te_{80}$ liquid, the simulation without dispersion forces [green curve in Fig. 4(c)] leads to a systematic increase of n_{GeTe} [broken line in Fig. 6(a)] while also increasing the distance at which $g_{GeTe}(r)$ is minimum from $r_{min} = 3.31$ Å to 3.53 Å. Using such simulations, one needs a cutoff distance of about 3.20 Å to obtain a value of $n_{GeTe} = 4$ [Fig. 6(a)], whereas the value of n_{GeTe} at $r_{min} = 3.53$ Å will lead to a substantially higher value for the coordination number (4.68). Furthermore, once the bond distance problem is solved using the dispersion correction of Eq. (1), this distance of 3.2 Å now appears to lie on the right tail of the first peak in $g_{GeTe}(r)$, and certainly not at its minimum [see also Fig. 5(a)].

Overall, the present calculations using dispersion forces improve the short-range structure of Ge-Te compounds featuring more structured liquids with much shorter bond distances as compared to previous simulations [31,32], and a well-defined first shell of Ge and Te neighbors, bringing not only pair correlation functions in much better agreement with experiments but also reducing the coordination numbers. Although there is a general agreement [18,19] on the fact that the coordination numbers of these systems are not governed by the "8-N bonding rule" (with N being the total number of s and p electrons in the outer shell of atoms), the fact that the first peak of the simulated total correlation function $g(r)$ has been up to now always found to be broader and shifted to higher interatomic distances [31,32] has led to a systematic overestimation of such coordination numbers.

C. Neighbor distribution

From the detailed analysis of neighbors (Table III), further insight into the network topology and its change with composition and temperature can be obtained by following the coordination distributions Ge^l and Te^l (l = I,II,III,IV,V,VI), these quantities being defined as the average number of atoms of a given species (Ge,Te) that are l-fold coordinated.

In these Ge-Te liquids, the dominant coordination is Ge^{IV} and Ge^{V}, and twofold, threefold, and fourfold tellurium, a result (Table III) that is consistent with the average value n_{Ge} and n_{Te} determined previously. At low Ge content ($Ge_{10}Te_{90}$) and high temperature (923 and 823 K), the liquid structure is composed of a majority of fourfold and fivefold germanium with a non-negligible fraction of sixfold Ge (11.5%–13.6%) in octahedral symmetry (see below). This fraction tends to decrease (4.5%) at the lowest temperature (700 K), and a conversion of germanium from sixfold into fourfold coordination is observed, accompanied by a moderate decrease of fivefold Ge. Similarly, one remarks that for tellurium the lower coordination (Te^{II}) grows at the expense of fourfold Te which decreases from 23.5% to 16.2% between 923 and 700 K. These trends are more or less recovered for the other compositions. When followed along an isotherm, the increase of composition affects the Ge environment and leaves the Te-based coordination distribution nearly unchanged between 10% and 15% Ge. Indeed, increasing the Ge content essentially increases the proportion of fourfold germanium and tends to reduce the fraction of higher coordinated species (e.g., 13.6% for $Ge_{10}Te_{90}$ against 4.2% for $Ge_{20}Te_{80}$) while also promoting threefold Ge.

Once again, in order to highlight some more general trends with composition, we focus on the effect of the chosen cutoff distance r_c that usually serves to determine the coordination distribution. Figure 7 shows the population of the most relevant coordination species as a function of r_c, and it appears that changes in coordination are moderate when r_c is slightly changed (e.g., ± 0.05 Å). More importantly, one can notice that the effect of composition on the statistical dependence with r_c is especially weak regarding the Ge population which shows virtually no change between $Ge_{10}Te_{90}$ [broken lines in Fig. 7(a)] and $Ge_{20}Te_{80}$ (solid lines). This means that the determination of the coordinations is mostly driven by the

TABLE III. Calculated coordination distribution at different temperatures. The cutoff has been taken at each respective minimum of the pair distribution function $r_{min} = 3.41$, 3.42, and 3.34 Å for $Ge_{10}Te_{90}$ at 923, 823, and 700 K, respectively; $r_{min} = 3.39$, 3.37, and 3.32 Å for $Ge_{15}Te_{85}$ at 923, 823, and 700 K, respectively, and $r_{min} = 3.30$, 3.28, and 3.31 Å for $Ge_{20}Te_{80}$ at 923, 823, and 700 K, respectively.

T (K)	Composition		I	II	III	IV	V	VI
923 K	$Ge_{10}Te_{90}$	Ge			8.2	46.0	34.3	11.5
823 K					3.5	45.8	37.1	13.6
700 K				0.2	4.8	61.8	28.7	4.5
923 K	$Ge_{15}Te_{85}$	Ge		0.2	6.6	51.4	32.3	9.5
823 K				0.1	5.2	48.2	35.2	11.3
700 K				0.3	8.3	67.2	21.3	2.9
923 K	$Ge_{20}Te_{80}$	Ge		0.8	10.4	52.7	29.3	6.8
823 K				0.8	11.2	60.5	23.2	4.3
700 K				0.3	5.6	55.9	31.4	6.8
923 K	$Ge_{10}Te_{90}$	Te	2.2	25.7	42.1	23.5	5.8	0.7
823 K			1.2	17.9	40.3	30.1	9.2	1.3
700 K			2.7	35.4	43.3	16.2	2.3	0.1
923 K	$Ge_{15}Te_{85}$	Te	2.4	27.5	42.3	22.3	5.0	0.5
823 K			2.2	25.2	41.2	24.3	6.3	0.8
700 K			3.0	38.2	42.5	14.3	1.9	0.1
923 K	$Ge_{20}Te_{80}$	Te	4.5	35.1	41.0	16.4	2.8	0.2
823 K			4.3	44.2	39.2	10.9	1.3	0.1
700 K			3.0	35.5	42.4	16.5	2.4	0.2

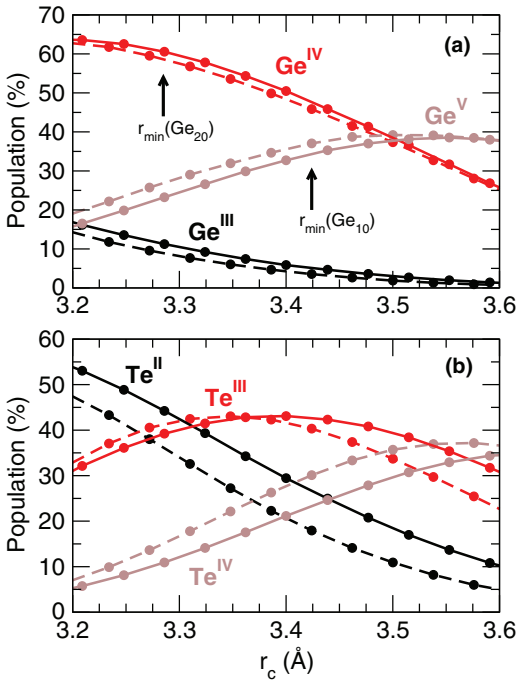

FIG. 7. (Color online) Effect of the cutoff distance r_c on the species population (in %) at 823 K for $Ge_{10}Te_{90}$ (broken lines) and $Ge_{20}Te_{80}$ (solid lines). (a) Population Ge^{III}, Ge^{IV}, and Ge^{V}. (b) Population Te^{II}, Te^{III}, and Te^{IV}. The arrows indicate the cutoff distance used for the computation of the coordination distribution of Table III, and which correspond to the minimum r_{min} of $Ge_{20}Te_{80}$ and $Ge_{10}Te_{90}$ in the corresponding pair distribution function (Fig. 4).

shift with composition of the minimum position r_{min} of the pair correlation function which changes from 3.42 to 3.28 Å between the $Ge_{10}Te_{90}$ and $Ge_{20}Te_{80}$ (see caption of Table III). Given that the experimentally determined minimum distances r_{min} of $g(r)$ are equal to 3.26 Å (Fig. 4) for both compositions, we have an estimation of the degree of error that is associated with such kind of calculation. For the $Ge_{20}Te_{80}$, one can have full confidence in the Ge coordination distribution given that the experimental r_{min} and chosen cutoff r_c nearly coincide, whereas the determined population of Ge coordinations in $Ge_{10}Te_{90}$ is biased by the difference in the minimum position r_{min} of the experimental and calculated pair correlation function $g(r)$. The same conclusions are encountered for the Te-based coordination distributions [Fig. 7(b)] which furthermore show strong effects with composition when the population is represented as a function of r_c.

D. Bond angles

Figures 8 and 9 show the most relevant bond angle distributions, and display their behavior with either composition (along the isotherm 823 K) or temperature (for the $Ge_{20}Te_{80}$ compound). The bond angle distribution Te-Te-Te is found to be weakly affected by a change in Ge content and temperature, as it displays the same shape associated with a defect octahedral geometry that leads to a dominant contribution at 90° and a minor one at $\simeq$ 160°. No changes are found when compared to the same distribution [33] for elemental Te (T = 970 K), indicating that the angles involved in such Te-Te-Te chain fragments are weakly affected by the Ge-induced crosslinking of the structure, even for the Ge-rich composition $Ge_{20}Te_{80}$. Similar results are found for bond angle distributions involving a Ge atom (Te-Te-Ge), which displays again the same contributions at $\simeq$90° and 160°. The latter (Te-Te-Ge) has an additional contribution at $\simeq$60° that we identify from a visual inspection of the atomic structure with angles defined by three atoms found within the equatorial plane of a Te-centered defective octahedra. Finally, we note a small change in the Ge-Te-Ge bond angle distribution (Fig. 8) with a slight increase between $Ge_{10}Te_{90}$ and $Ge_{15}Te_{85}$ from contributions of 80° but this difference could also arise from the small statistics given the limited number of Ge atoms at smaller compositions.

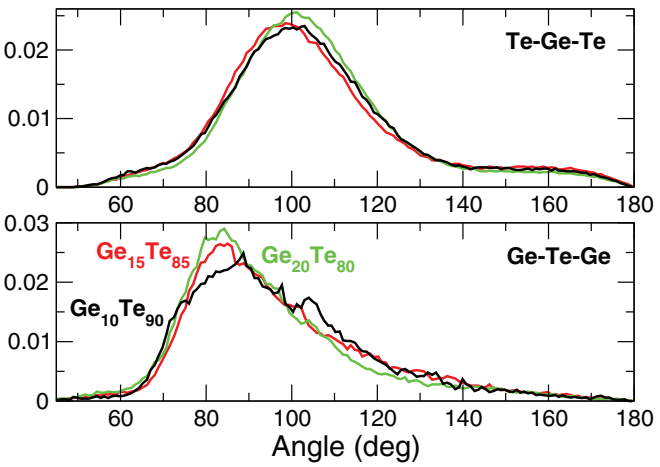

FIG. 8. (Color online) Te-Ge-Te and Ge-Te-Ge bond angle distributions at 823 K for the three compositions $Ge_{10}Te_{90}$ (black), $Ge_{15}Te_{85}$ (red), and $Ge_{20}Te_{80}$ (green). Note that the Te-Te-Te and Te-Te-Ge bond angle distributions of $Ge_{10}Te_{90}$ and $Ge_{15}Te_{85}$ (not shown) have exactly the same shape as $Ge_{20}Te_{80}$ (see Fig. 9).

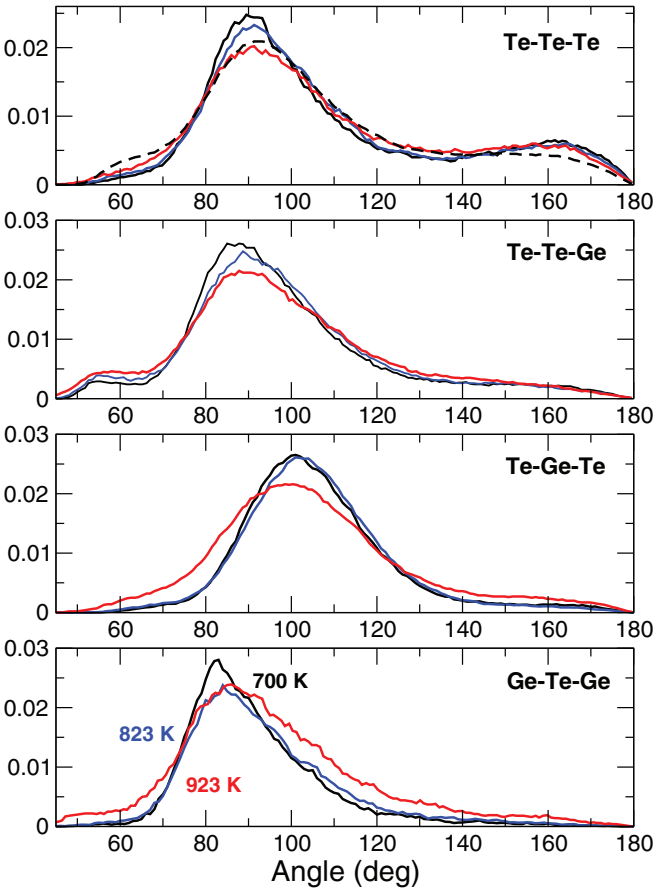

FIG. 9. (Color online) Te-Te-Te, Te-Te-Ge, Te-Ge-Te, and Ge-Te-Ge bond angle distributions and $Ge_{20}Te_{80}$ liquid at the three temperatures: 923 K (red), 823 K (blue), and 700 K (black). The broken line in the top panel (Te-Te-Te) is the computed bond angle distribution of a 970-K simulated liquid Te (see text for details).

More changes appear when the bond angle is followed (Fig. 8) with temperature at a given composition $Ge_{20}Te_{80}$, this being particularly visible for the bond angle distributions involving a Ge atom. With decreasing temperature, the shift to higher angles between 923 and 823 K of the distribution Te-Ge-Te is a direct indication that the average fraction of tetrahedral sites is increasing as already emphasized from the evolution of the order parameter S. Similarly, the sharpening of Ge-Te-Ge distribution indicates the tendency towards an increased well-defined environment.

V. VIBRATIONAL AND ELECTRONIC DENSITY OF STATES

The vibrational density of states (VDOS) $g(\omega)$ of the different Ge-Te liquids is represented in Fig. 10 for selected temperatures, and compared to our experimental measurements, using the Fourier transform of the velocity-velocity

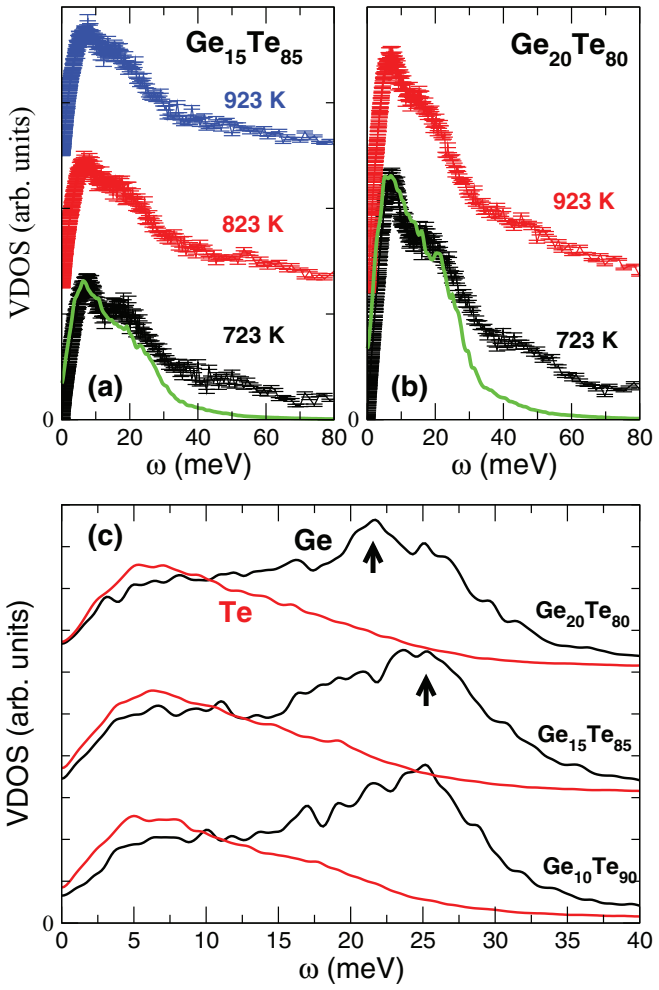

FIG. 10. (Color online) Computed and experimental vibrational density of states (VDOS) in Ge-Te liquids. (a) Experimentally measured VDOS of $Ge_{15}Te_{85}$ at 723 K (black), 823 K (red), and 923 K (blue), compared to the computed VDOS at 700 K (green curve). (b) Measured VDOS of $Ge_{20}Te_{80}$ at 723 K (black) and 923 K (red), compared to the computed VDOS at 700 K (green curve). (c) Computed partial contribution (Ge, black and Te, red) to the VDOS at 700 K.

autocorrelation function

$$g(\omega) = \frac{1}{Nk_BT}\sum_{j=1}^{N}\int_{-\infty}^{\infty}\langle \mathbf{v}_j(t)\mathbf{v}_j(0)\rangle e^{i\omega t}dt. \qquad (5)$$

We remark that the low-frequency region of the VDOS is very well reproduced [Figs. 10(a) and 10(b)] and consists for both investigated systems ($Ge_{15}Te_{85}$ and $Ge_{20}Te_{80}$) in a main peak centered at $\simeq$10 meV, together with a shoulder at slightly higher frequency ($\simeq$20 meV) followed by a decrease. The calculated VDOS actually reproduce with a reasonable agreement the VDOS at low frequency ($E < 30$ meV) but decreases much more rapidly to zero at higher frequency. We remind that since the available $E = \hbar\omega$ range is correlated with a finite k range, $g(\omega)$ is incomplete and slightly distorted. In this respect, the shapes of both experimental and theoretical curves are quite similar to those obtained in a study on different tellurides [36].

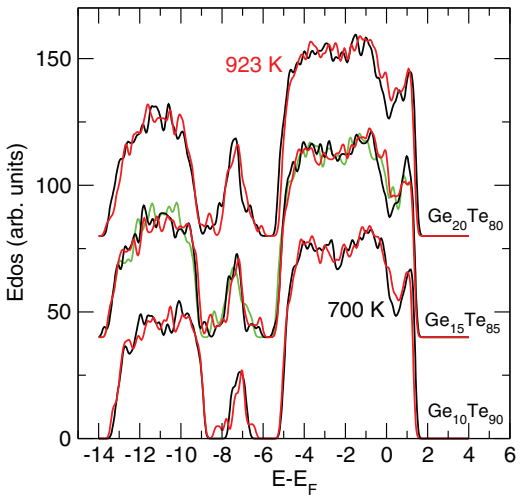

FIG. 11. (Color online) Computed electronic density of states of liquid (700 K, black and 923 K, red) $Ge_{10}Te_{90}$, $Ge_{15}Te_{85}$, and $Ge_{20}Te_{80}$ alloys. The green curve is a calculation without the dispersion correction of Eq. (1).

The structure of the contribution at $\simeq$25 meV changes in an important fashion with composition as seen from the partial contributions [Fig. 10(c)]. The peak associated with Ge-based vibrations shifts indeed to lower frequencies [arrows in Fig. 10(c)].

Figure 11 shows the electronic density of states (EDOS) of the three compositions at two different temperatures (700 and 923 K). The computation has been performed over five independent configurations of each liquid composition, prior to a wave-function optimization and an eigenvalue (Kohn-Sham energies) calculation. We notice that the global profile remains nearly the same for all compositions with mainly two s bands between -14 and -6.0 eV, well separated from the valence p-band structure. However, the minimum at the Fermi energy becomes more pronounced as the temperature is decreased from 923 to 700 K. Effects of composition are essentially visible in the 4s Ge band located at $\simeq -7$ eV which shows an increase in intensity as the liquid evolves from $Ge_{10}Te_{90}$ to $Ge_{20}Te_{80}$.

These trends are consistent with earlier findings [40], and it should be noted that the absence of the dispersion correction of Eq. (1) does not modify the global shape but tends to reduce the pseudogap at the Fermi energy, a result that seems consistent with the reduction of the bond lengths which lead to a more localized electronic structure.

VI. CONCLUSIONS

Liquids belonging to the Ge-Te family are not only at the basis of important optoelectronic applications when alloyed with appropriate elements, they also display a variety of intriguing phenomena among which is the so-called "*density anomaly*" [29]. The understanding of these phenomena and the description of their properties including their structure is the subject of intense research.

Here, we have studied the structure of three compositions in the Ge-Te binary by combining molecular simulations, neutron

diffraction, and inelastic neutron scattering experiments. We have focused on three target compositions $Ge_{10}Te_{90}$, $Ge_{15}Te_{80}$, and $Ge_{20}Te_{80}$ and three temperatures (923, 823, and 700 K). Such systems have been studied for quite some time in the literature but only at low temperature in the amorphous phase, or restricted to a single composition (essentially the eutectic $Ge_{15}Te_{85}$). Here, Ge-Te liquids are studied in a systematic fashion under temperature and Ge content change, in a combined effort using both theory and experiments. With respect to previous studies on the same systems [31,32], this study furthermore marks a clear improvement when both simulated and experimental structural properties are compared. This is especially appealing from the agreement obtained in the reproduction of the pair correlation function in real space, and the structure factor in reciprocal space, this statement being valid for all compositions and temperatures. We identify the origin of the improvement in the account of a dispersion (Grimme) correction [61] which handles in a semiempirical way effects of polarizability that contribute to Van der Waals forces. As a general result, most typical bond distances of Ge-Te liquids are reproduced with confidence, among which the distance corresponding to the first peak of the pair correlation function $g(r)$, identified with contributions coming from both Ge-Te and Te-Te bonds.

Regarding structural properties, our first-principles model shows that the coordination numbers are decreased with respect to previous findings, a result that arises not only from the fact that the first peak in $g(r)$ is reproduced with a very good accuracy, but also from the calculated value of the first minimum of the pair correlation function which is now found to be very close to its experimental counterpart. At all compositions and for all temperatures, the structure is made of a majority of Ge in defective octahedral geometry as detected from the bond angle distributions, with coordination numbers between 3 and 6, whereas tellurium is found to have mostly a large amount of twofold and threefold atoms, the former increasing with decreasing temperature at the expense of the latter.

Given these results, what are the broader perspectives of this work? Obviously, taking into account dispersion forces in molecular simulations resolves the well-known bond distance problem encountered in all previous DFT-based simulations of amorphous or liquid tellurides. It is not clear at this stage if such improvements will remain at low temperatures once the liquids have been quenched to the glass, but it suggests that similar telluride liquids may be improved using the same scheme. As a final comment, it should be emphasized that the way these attractive forces affect the structure is not straightforward. In fact, they are only effective at large distances when the damping function is active ($r > R_c = 3.45$ Å) but they essentially improve the short-range structure and solve the bond distance problem, while leaving structural correlations at larger distances ($r > R_c$) nearly unchanged.

ACKNOWLEDGMENTS

The authors thank P. Boolchand, K. Gunasekera, A. Kachmar, M. Boero, S. Le Roux, C. Massobrio, and R. Vuilleumier for useful and stimulating discussions. Support from Agence Nationale de la Recherche (ANR) (Grant No. ANR-11-BS08-0012) is gratefully acknowledged. GENCI (Grand Equipement National de Calcul Intensif) is acknowledged for supercomputing access. M.M. acknowledges support from the Franco-American Fulbright Commission, and International Materials Institute (H. Jain) for financial support.

[1] A. A. Wilhelm, C. Boussard-Plédel, Q. Coulombier, J. Lucas, B. Bureau, and P. Lucas, Adv. Mater. **19**, 3796 (2007).
[2] M. C. Kum, H. S. Jung, N. Chartuprayoon, W. Chen, A. Mulchandani, and N. V. Myung, J. Phys. Chem. C **116**, 9202 (2012).
[3] *Amorphous Chalcogenides*, edited by V. I. Mikla (Elsevier, Amsterdam, 2012).
[4] K. Tanaka, Phys. Status Solidi B **250**, 988 (2013).
[5] P. Chen, C. Holbrook, P. Boolchand, D. G. Georgiev, K. A. Jackson, and M. Micoulaut, Phys. Rev. B **78**, 224208 (2008).
[6] R. Lukacs and S. Kugler, Jpn. J. Appl. Phys. **50**, 091401 (2011)
[7] D. G. Georgiev, P. Boolchand, and M. Micoulaut, Phys. Rev. B **62**, R9228 (2000).
[8] A. A. A. El-Rahman, A. M. Eid, M. Sanad, and R. M. El-Ocker, J. Phys. Chem. Solids **59**, 825 (1998).
[9] Y. Wang, P. Boolchand, and M. Micoulaut, Europhys. Lett. **52**, 633 (2000).
[10] Z. Yang and P. Lucas, J. Am. Ceram. Soc. **92**, 2920 (2009).
[11] Z. Yang, A. A. Wilhelm, and P. Lucas, J. Am. Ceram. Soc. **93**, 1941 (2010).
[12] V. T. Mai, R. Escalier, C. Vigreux, and A. Pradel, Thin Solid Films **524**, 309 (2012).
[13] C. Vigreux, E. Barthélémy, L. Bastard, J.-E. Broquin, S. Ménard, M. Barillot, G. Parent, and A. Pradel, Opt. Mater. Express **1**, 357 (2011).
[14] P. Lucas, Z. Yang, M. K. Fah, T. Luo, S. Jiang, C. Boussard-Pledel, M.-L. Anne, and B. Bureau, Opt. Mater. Express **3**, 1049 (2013).
[15] C. Vigreux-Bercovici, E. Bonhomme, and A. Pradel, J. Non-Cryst. Solids **353**, 1388 (2007).
[16] C. Vigreux-Bercovici, E. Bonhomme, A. Pradel, J.-E. Broquin, L. Labadie, and P. Kern, Appl. Phys. Lett. **90**, 011110 (2007).
[17] S. Danto, P. Houizot, C. Boussard-Plédel, X. H. Zhang, F. Smektala, and J. Lucas, Adv. Funct. Mater. **16**, 1847 (2006).
[18] *Phase Change Materials and Applications*, edited by S. Raoux, and M. Wuttig (Springer, Berlin, 2008).
[19] S. Raoux, W. Wełnic, and D. Ielmini, Chem. Rev. **110**, 240 (2010).
[20] D.-H. Lee, C.-P. Hong, and S.-D. Kim, Lect. Notes Electr. Eng. **215**, 433 (2013).

[21] J. K. Olson and H. Li, and P. C. Taylor, J Ovonics Res. **1**, 1 (2005).
[22] D. A. Baker, M. A. Paesler, G. Lucovsky, S. C. Agarwal, and P. C. Taylor, Phys. Rev. Lett. **96**, 255501 (2006).
[23] Y. Tsuchiya, J. Phys. Soc. Jpn. **57**, 3851 (1988).
[24] Y. Tsuchiya, J. Phys.: Condens. Matter **4**, 4335 (1992).
[25] D. Chandra and L. R. Holland, J. Vac. Sci. Technol. A **1**, 1620 (1983).
[26] V. M. Glazov, S. N. Chizhevskaia, and N. N. Glagoleva, *Liquid Semiconductors* (Plenum, New York, 1969).
[27] Y. Tsuchiya (private communication).
[28] Y. Tsuchiya, J. Non-Cryst. Solids **136**, 37 (1991).
[29] Y. Tsuchiya, J. Phys. Soc. Jpn. **60**, 227 (1991).
[30] H. Turn and J. Ruska, J. Non-Cryst. Solids **22**, 331 (1976).
[31] C. Bichara, M. Johnson, and J.-Y. Raty, Phys. Rev. Lett. **95**, 267801 (2005).
[32] J. Akola and R. O. Jones, Phys. Rev. Lett. **100**, 205502 (2008).
[33] C. Bergman, C. Bichara, J.-P. Gaspard, and Y. Tsuchiya, Phys. Rev. B **67**, 104202 (2003).
[34] M.-V. Coulet, D. Testemale, J. L. Hazemann, J. P. Gaspard, and C. Bichara, Phys. Rev. B **72**, 174209 (2005).
[35] J. Akola, R. O. Jones, S. Kohara, T. Usuki, and E. Bychkov, Phys. Rev. B **81**, 094202 (2010).
[36] C. Otjacques, J.-Y. Raty, M.-V. Coulet, M. Johnson, H. Schober, C. Bichara, and J.-P. Gaspard, Phys. Rev. Lett. **103**, 245901 (2009).
[37] S. Caravati, M. Bernasconi, and M. Parrinello, Phys. Rev. B **81**, 014201 (2010).
[38] C. Otjacques, J.-Y. Raty, F. Hippert, H. Schober, M. Johnson, R. Ceolin, and J.-P. Gaspard, Phys. Rev. B **82**, 054202 (2010).
[39] S. Caravati, M. Bernasconi, T. D. Küehne, M. Krack, and M. Parrinello, Appl. Phys. Lett. **91**, 171906 (2007).
[40] J. Akola and R. O. Jones, Phys. Rev. B **76**, 235201 (2007).
[41] C. Bichara, M. Johnson, and J.-P. Gaspard, Phys. Rev. B **75**, 060201 (2007).
[42] A. Menelle, R. Bellissent, and A. M. Flank, Europhys. Lett. **4**, 705 (1987).
[43] H. Neumann, W. Matz, W. Hoyer, and M. Hobst, Phys. Status Solidi **90**, 489 (1985).
[44] P. Jóvári, I. Kaban, W. Hoyer, R. G. Delaplane, and A. Wannberg, J. Phys.: Condens. Matter **17**, 1529 (2005).
[45] M. Micoulaut, A. Kachmar, M. Bauchy, S. Le Roux, C. Massobrio, and M. Boero, Phys. Rev. B **88**, 054203 (2013).
[46] C. Massobrio, M. Celino, P. S. Salmon, R. A. Martin, M. Micoulaut, and A. Pasquarello, Phys. Rev. B **79**, 174201 (2009).
[47] M. Bauchy, M. Micoulaut, M. Celino, S. Le Roux, M. Boero, and C. Massobrio, Phys. Rev. B **84**, 054201 (2011).
[48] A. V. Kolobov, P. Fons, A. I. Frenkel, A. L. Ankudinov, J. Tominaga, and T. Uruga, Nat. Mater. **3**, 703 (2004).
[49] W. Wełnic, A. Pamungkas, R. Detemple, C. Steimer, S. Blügel, and M. Wuttig, Nat. Mater. **5**, 56 (2006).
[50] J. Kalikka, J. Akola, R. O. Jones, S. Kohara, and T. Usuki, J. Phys.: Condens. Matter **24**, 015802 (2012).
[51] E. Cho, J. Im, C. Park, W. J. Son, D. H. Kim, H. Horii, J. Ihm, and S. Han, J. Phys.: Condens. Matter **22**, 205504 (2010).
[52] M. Micoulaut, A. Kachmar, and Th. Charpentier, Phys. Status Solidi B **249**, 1890 (2012).
[53] M. Micoulaut, J. Chem. Phys. **138**, 061103 (2013).
[54] J. P. Itié, A. Polian, G. Calas, J. Petiau, A. Fontaine, and H. Tolentino, Phys. Rev. Lett. **63**, 398 (1989).
[55] CORRECT: A correction program for neutron diffraction data, Version 2.4, M. A. Howe, R. L. McGreevy, and P. Zetterström, 1998.
[56] H. Fischer, A. C. Barnes, and P. S. Salmon, Rep. Prog. Phys. **69**, 233 (2006).
[57] LAMP, the large Array Manipulation Program. http://www.ill.fr/data_treat/lamp/the_lamp-book.
[58] CPMD, http://www.cpmd.org.
[59] N. Trouillier and J. L. Martins, Phys. Rev. B **43**, 1993 (1991).
[60] S. Nosé, Mol. Phys. **52**, 255 (1984); W. G. Hoover, Phys. Rev. A **31**, 1695 (1985).
[61] S. Grimme, J. Comput. Chem. **27**, 1787 (2006).
[62] R. Jonchière, A. P. Seitsonen, G. Ferlat, A. M. Saitta, and R. Vuilleumier, J. Chem. Phys. **135**, 154503 (2011).
[63] C. Steimer, V. Coulet, W. Wełnic, H. Dieker, R. Detemple, C. Bichara, B. Beuneu, J. P. Gaspard, and M. Wuttig, Adv. Mater. **20**, 4535 (2008).
[64] We relate the position r of a peak in real space to the position k of a corresponding peak in Fourier space by using the relation $k \cdot r \approx 7.7$, which identifies the location of the first maximum of the spherical Bessel function $j_0(kr)$.
[65] P. Jóvári, A. Piarristeguy, R. Escalier, I. Kaban, J. Bednarčik, and A. Pradel, J. Phys.: Condens. Matter **25**, 195401 (2013).
[66] *Landolt-Börnstein New Series I/16A*, edited by Ed Schopper (Springer, Berlin, 2000).
[67] L. Pauling, *Nature of the Chemical Bond* (Cornell University Press, Ithaca, NY, 1960).
[68] H. Endo, K. Maruyama, H. Hoshino, and H. Ikemoto, Z. Phys. Chem. **217**, 863 (2003).
[69] J. Y. Raty, J. P. Gaspard, and C. Bichara, J. Phys.: Condens. Matter **15**, S167 (2003).
[70] M. Micoulaut, J. Phys.: Condens. Matter **16**, L131 (2004).